Research papers

Novel dual-mixed refrigerant precooling process for high capacity hydrogen liquefaction plants with superior performance

Ahmad K. Sleiti [*], Wahib A. Al-Ammari , Saud Ghani

Department of Mechanical & Industrial Engineering, College of Engineering, Qatar University, Doha, Qatar

A B S T R A C T

Liquid hydrogen is a superior alternative for the current energy storage methods and energy carriers as it has higher energy density and cleanliness. However, hydrogen liquefaction is an energy-intensive process. In particular, the precooling process of hydrogen consumes a tremendous portion of about 30 % of the total compression power of the plant. Several previous studies introduced various pure-refrigerant and single mixed refrigerant (SMR) precooling processes, however, their specific energy consumption (SEC) still very high especially at large-scale capacities. Therefore, this study presents a novel, efficient, and large-scale dual-mixed refrigerant (DMR) process to precool the hydrogen from 25 °C to -192 °C at a pressure of 21 bar. New heavyweight-based mixed refrigerant MR1 and lightweight-based mixed refrigerant MR2 are developed for the DMR process using a new-proposed systematic approach. The proposed DMR process is capable of handling a wide range of hydrogen flow from 100 TPD to 1000 TPD with SEC of 0.862 kWh/kgH$_{2\text{Feed}}$, which is 20.33 % lower than the most competitive SMR process available in the literature. Based on the sensitivity analysis, further optimization of the DMR operating parameters reduced the SEC to 0.833 kWh/kgH$_{2\text{Feed}}$ at an optimal capacity of 500 TPD. Furthermore, the COP of the new process is improved by 14.47 % and the total annualized cost is reduced by 12.24 %. Compared to five other technologies that use the pure-refrigerant and other SMR precooling processes, the DMR reduces the SEC by 39.0 % to 63.0 %. The novel precooling process presented herein has the potential to drive the development of large-scale hydrogen liquefaction processes.

1. Introduction

Liquid hydrogen is a superior alternative for the current energy storage methods and energy carriers as it has higher energy density (on mass basis ~120 MJ/kg) and cleanliness [1]. The transition to the hydrogen as the fuel of the future is imposed by the severe global warming problem that threatens the survival and development of mankind [2,3]. For instance, it is reported that from 2021 to 2050, the use of hydrogen can avoid 80 gigatons of cumulative CO$_2$ emissions. In addition, hydrogen will contribute towards 20 % of the total abatement needed in 2050 [4]. Liquid hydrogen (LH$_2$) is a more cost-effective way to transport hydrogen over long distances than compressed gas for several reasons [5,6]. Firstly, the volumetric density of LH$_2$ is much higher than that of compressed hydrogen. At 1 bar and -253 °C, the volumetric density of LH$_2$ is 70 kgH$_2$/m3, which is three times higher than the average density of compressed hydrogen, which is 21 kgH$_2$/m3 at 700 bar and 25 °C. Secondly, compressed gas poses significant safety risks, including the potential for explosions in the event of material

failure or storage penetration. Thirdly, the cost of hydrogen storage in liquid form is 6 $/kWh compared to 15 $/kWh in compressed form at 700 bar or 13 $/kWh at 300 bar [7]. Moreover, the world's first LH$_2$ carrier ship was launched by HySTRA partners (Kawasaki Heavy Industries, Iwatani Crop & Shell) in Japan in 2019. The ship has a carrying capacity of 75 bar and was used as a prototype to demonstrate voyages between Australia and Japan, ushering in the LH$_2$ economy. In addition, LH$_2$ have a great potential as an energy storage method to solve the intermittency issue of the renewable energy sources that reduces their capacity by 20 % to 40 % [8,9]. Furthermore, LH$_2$ systems can be utilized for peak shaving during energy shortages [10]. Peak shaving refers to the practice of reducing peak energy demand by utilizing alternative energy sources or reducing energy consumption during periods of high energy usage. In the context of LH$_2$ systems, peak shaving can be achieved by utilizing stored liquid hydrogen to generate electricity during periods of high demand, thereby reducing the need for conventional energy sources such as coal or natural gas. However, while LH$_2$ transportation is more economically feasible than compressed gaseous form, its liquefaction process is still highly cost intensive (capital cost of about

---

Nomenclature

Symbol	
A	capacity parameter
C_{BM}	base module cost, ($)
COP	coefficient of performance of the precooling process
$\dot{E}$	exergy rate, (kW)
$\dot{G}$	Gibbs free energy rate, (kW)
h	specific enthalpy, (kJ/kg)
$\dot{m}$	mass flow rate, (kg/s)
$P_{h,MR1}$	high-pressure of the first mixed refrigerant, (bar)
$P_{h,MR2}$	high-pressure of the second mixed refrigerant, (bar)
$P_{l,MR1}$	low-pressure of the first mixed refrigerant, (bar)
$P_{l,MR2}$	low pressure of the second mixed refrigerant, (bar)
Q	heat transfer rate, (kW)
SEC	specific energy consumption, (kWh/kgH$_{2Feed}$)
$\dot{W}$	power generation/consumption rate, (kW)
ε	exergy efficiency, (%)
Subscripts	
i	for stream$_i$

in	at the inlet
j	for component j
o	at ambient conditions
out	at outlet
Abbreviations	
CL	cooler
DMR	dual mixed-refrigerant
Exp.	liquid expander
EV	expansion valve
GRC	grass root cost
HF	hydrogen feed gas
HX	heat exchanger
LNG	liquefied natural gas
MR	mixed refrigerant
OC	operational costs
PBP	payback period
SMR	single mixed-refrigerant
TAC	total annualized cost

9000 $/kg$_{LH2}$) [11] and consumes large amount of energy for operation (10–13 kWh/kg$_{LH2}$) compared to a minimum theoretical energy consumption of 3.30 kWh/kg$_{LH2}$ [12].

The existing hydrogen liquefaction plants consume about 10–13 kWh/kg$_{LH2}$ at capacities between 5 and 35 TPD (tons per day) [11,12]. All of these plants use the pre-cooled Claude system as developed 55 years ago with minor improvements. The Claude cycle is a process that utilizes hydrogen as the working medium. The hydrogen undergoes compression, cooling, and expansion through a Joule-Thomson Valve. A part of the compressed hydrogen gas is expanded in an expansion turbine to generate colder gas. This colder gas is then combined with saturated vapor from the flash end separator. This mixture is used to cool the compressed hydrogen gas. Other conceptual large-scale liquefaction processes, which are discussed in the next paragraph, were proposed that consume 6 to 11 kWh/kg$_{LH2}$ (which means 20 % to 33 % of the energy carried by the produced LH$_2$ is consumed) at capacities between 170 TPD to 300 TPD such as reported in [13]. However, these processes still energy intensive, suffer from complexity, and need significant further improvements in the selection of their mixed refrigerants. This is essential step to make the LH$_2$ commercially competitive to the liquid natural gas (LNG) from energetic and economic point of views.

Hydrogen liquefaction process is mainly composed of two major stages, namely the pre-cooling process, and the liquefaction process. Typically, in the precooling-stage, the feed hydrogen flow is cooled from 25 °C to -193 °C and from -193 °C to -253 °C in the liquefaction stage. Several liquefaction cycles were introduced including: (a) nitrogen precooled cycles [14,15], (b) helium precooled cycles [16,17], (c) liquefied natural gas (LNG) precooled cycles [18,19], (d) Joule-Brayton (J-B) precooled cycles [20], (e) Joule-Thomson precooled cycles [21], and (f) mixed refrigerant (MR) precooled cycles in standalone [22,23] or integrated [24,25] structures. In these cycles, special focus is given to the precooling process because it is the stage with most degree of freedom in the design and consumes more than 30 % of the overall compression power. Other studies attempt to reduce the precooling energy consumption by integrating it with absorption refrigeration system [26], steam methane reforming and CO$_2$ liquefaction processes [27], and thermos-electrochemical water splitting cycle [28]. As reviewed by Liang and Yonglin [20], the average specific energy consumption (SEC) of the nitrogen and helium precooled cycles is 11.47 kWh/kg$_{LH2}$ which is 76 % higher than the J-B cycles (6.51 kWh/kg$_{LH2}$), and 89 % higher than the MR precooled cycles (6.06 kWh/kg$_{LH2}$). This is

mainly caused by the need for a liquid nitrogen or helium to perform the precooling process, which need extra plant to cool and liquefy them. For the LNG precooled cycle, the SEC was 4.00 kWh/kgLH$_2$, which is the lowest value of all precooled technologies. However, this value excludes the consumed energy to liquefy the natural gas itself. A In addition, the availability of LNG to perform the liquefaction process is not always feasible. Also, the use of LNG limits the precooling temperature to less than −162 °C. In contrast, the MR precooled cycles precool the hydrogen feed gas and the mixed refrigerants with minimal compression power (with suitable mixed refrigerant) and the precooling process could reach a temperature of −198 °C. Thus, the MR cycles for hydrogen liquefaction can potentially achieve lower SEC without losing their configuration simplicity (similar to those used in natural gas liquefaction [29,30]). To improve the performance of the MR precooled cycles, new configurations with new mixed refrigerants are introduces in the present study as summarized in the subsequent subsections.

In 2006, Stang et al. [31] introduced the first conceptual plant that uses mixed refrigerant for the H$_2$ precooling stage and liquid helium for the cryogenic section. They reported the feasibility of the process with exergy efficiency of 60 % and SEC of 7.0 kWh/kg$_{LH2}$. In 2010, Berstad et al. [13] presented a new hydrogen liquefaction process by replacing the cascade ethane and propane precooling process with mixed refrigerant process that precools the hydrogen from 25 °C to −198 °C with SEC of 1.74 kWh/kgH$_{2Feed}$. Also, in 2010, Krasae-In et al. [32] explained a large-scale LH$_2$ plant that use MR precooling process with overall power consumption of 5.35 kWh/kg$_{LH2}$ with 1.30 kWh/kg$_{LH2}$ is consumed in the precooling stage. The plant capacity was 100 TPD and the hydrogen is precooled from 25 °C to -193 °C. Then, in 2011, Krasae-In et al. experimentally tested a small-scale laboratory hydrogen liquefaction plant with MR precooling system. The feed hydrogen is cooled from 25 °C to -158 °C at flow rate of 0.60 kg/h with SEC of 1.76 kWh/kgH$_{2Feed}$. In 2017, Sadaghiani and Mehrpooya [33] introduced a large-scale MR precooled configuration with capacity of 300 TPD. The precooling section precools the hydrogen gas from 25 °C to -195 °C and has the least SEC (1.102 kWh/kg$_{LH2}$) compared to the other MR precooling process up to date. Most of the studies available on the literature analyzed the energy and exergy performance of the hydrogen MR precooled cycles [20,34,35]. However, the economic evaluation has not been ind in these studies except the exergeconoimic analysis presented by Ansarinasab et al. [36,37]. Moreover, the exergy efficiencies of the existing H$_2$ liquefaction plants is in the range of only 20 %–30 % [38].

Although in one proposed MR precooled cycle [20], the exergy efficiencies were boosted to the range of 40 %–60 %, however, significant further improvements still needed with focus on the exergetic performance of the cryogenic heat exchangers as they cause huge irreversibilities at the cryogenic temperatures [39].

All of the aforementioned MR precooled cycles use single mixed refrigerant (SMR) for the precooling process. However, the SMR limits the performance improvements of the heat exchangers in the precooling stage. Also, it contains significant portion of lightweight refrigerants, which increase the compression power. Significant improvements on the performance of the MR precooling process could be achieved by applying a dual-mixed refrigerants (DMR) for the precooling stage, which is the main objective of the present study. That is the available MR precooling process in the literature use single mixed refrigerant in a single circulation loop to perform the hydrogen precooling processes. In this study, two integrated circulation loops are constructed to perform the precooling process with a distinguished mixed refrigerant is used in each loop. This enables more flexibility on the composition of each refrigerant and leads to much lower SEC as discussed in Section 2. To the knowledge of the authors and based on exhaustive literature search, there is no study in open literature that investigates the utilization of dual-mixed refrigerants process for the precooling stage. Furthermore, the available MR processes lack economic evaluation as pointed earlier and the methodology behind the development of their mixed refrigerants is not mentioned. To address these gaps, the present study aims at:

- Proposing a novel dual-mixed refrigerant (DMR) precooling process with superior performance as replacement to the existing conventional and the SMR precooling processes used in hydrogen liquefaction plants.
- Developing new mixed refrigerants for the proposed process that achieve extraordinary performance from energetic and exergetic point of view.

- Presenting a systematic and new methodology for mixing refrigerants for the precooling process of hydrogen liquefaction.
- Conducting energetic, exergetic, economic, and environmental analyses for the proposed process. Also, thorough sensitive analysis and preliminary optimization are performed.
- Comparing the performance of the proposed DMR process with the other conventional and SMR processes available in literature.

It is worth mentioning that the authors have filed provisional patent [40] based on the finding of this article.

The rest of the manuscript is organized as following: Section 2 describes the typical conditions of the precooling and liquefaction process in the MR precooled cycles, the configuration of a SMR precooling process, which is selected as a reference case, and the detailed layout of the proposed DMR precooling process. Section 3 explains the methodology used to evaluate the energetic, exergetic, and economic performances of the present DMR and reference SMR precooling processes. Section 4 presents and discusses the results of both reference SMR and DMR processes followed by detailed sensitivity analyses and preliminary optimization for the proposed DMR process. The main findings and conclusions are provided in Section 5.

2. Description of the novel DMR precooling process for LH$_2$ plant

The liquefaction process of the hydrogen gas as depicted in Fig. 1 for both SMR and the proposed DMR has mainly two stages: precooling process, and liquefaction process. Note that large-scale flowsheets of the precooling processes for SMR and DMR are given in Fig. 2 and Fig. 3, respectively. The precooling process reduces the temperature of the feed hydrogen from the ambient temperature (25 °C) to a temperature of -195 °C at feed pressure of 21 bar. Then, the liquefaction process cools the hydrogen further from -195 °C to -253 °C at outlet pressure of 1.3 bar. In this study, a novel dual-mixed refrigerant (DMR) precooling
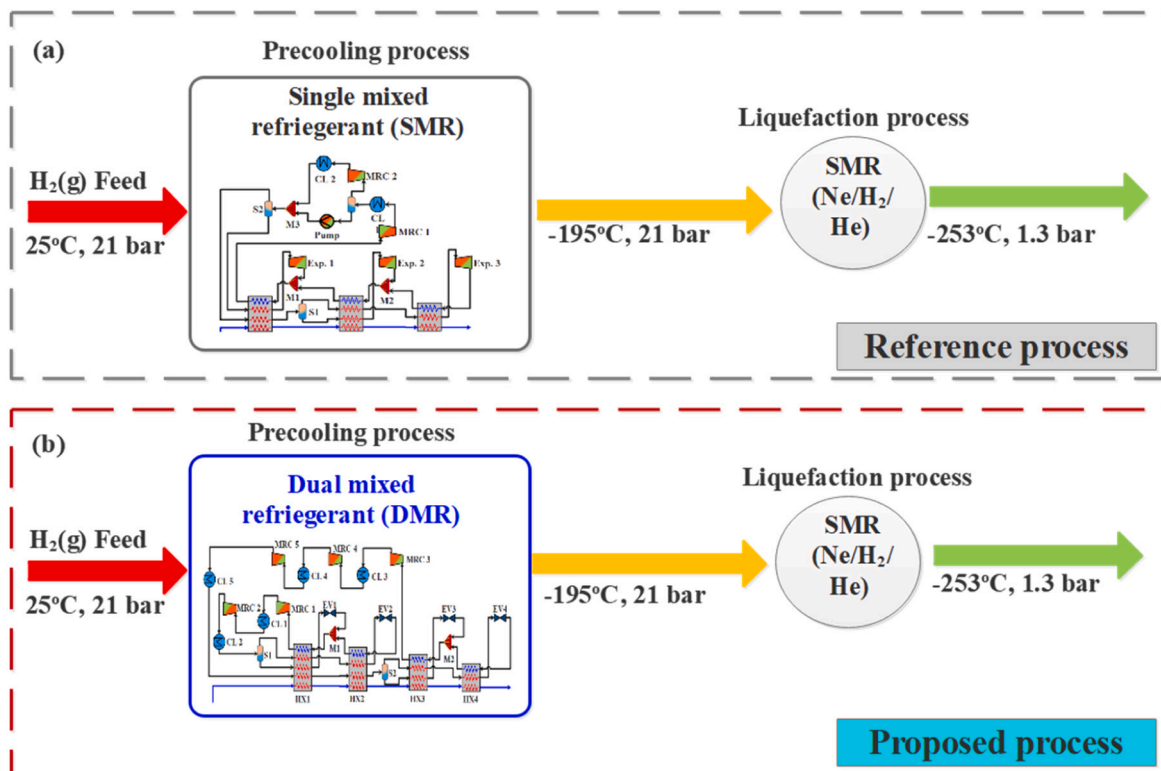

Fig. 1. Block flow diagram of the hydrogen liquefaction process using the configuration of (a) reference SMR precooling process [33], and (b) proposed DMR precooling process.
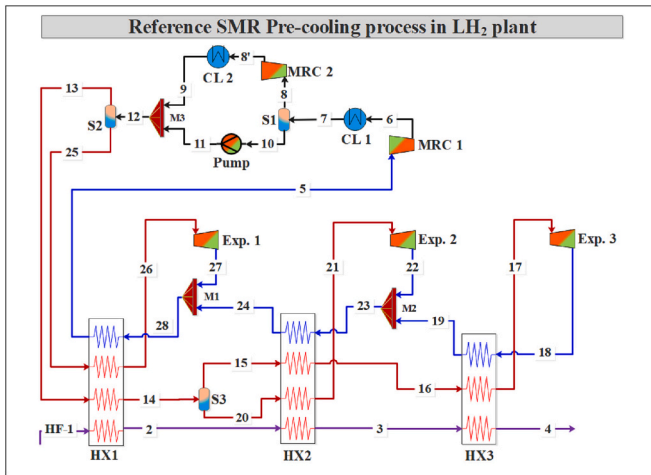
Fig. 2. Flowsheet of the reference SMR precooling process in LH2 plant which is introduced by [33].

process is developed to replace the single mixed refrigerant (SMR) precooling process developed by Sadaghiani and Mehrpooya [33].

With proper selection of the mixed refrigerants, the DMR process will potentially achieve superior performance compared to the SMR processes from energetic, exergetic, and economic point of views. This is because in the proposed DMR process, two classes of refrigerants are used; heavy refrigerants for its first loop and lighter refrigerants for the second loop, which efficiently reduces the compression power and subsequently the specific energy consumption of the process. Since heavy refrigerants have a higher molecular weight than light refrigerants, separating them into a distinct loop improves the efficiency of the compression process. Therefore, by using heavy refrigerants in the

first loop, the required compression power for this loop is reduced. Similarly, the use of light refrigerants in a separated loop enables them to provide the same cooling effect with a lower mass flow rate than if they were mixed with the heavy refrigerants. This also reduces the compression power required for the second loop. Furthermore, the cold-composite curves of the heat exchangers in the DMR can be improved to match the hot-composite curve with more flexibility than in SMR process. This, in turn, enhances the COP of the precooling process and reduces the exergy destruction rates as well. The efficient performance of the compressors and heat exchangers of the DMR process minimizes its capital and operational costs compared to the SMR or other pure-refrigerant precooling processes. The reduction of the total annualized cost of the DMR reaches about 12 % compared to that of the SMR as discussed in Section 4.3. All of these features of the DMR process over the SMR process are discussed in detail in section 4. The detailed description of the flowsheets of the reference SMR process and the proposed DMR are introduced in the next two subsections.

In this study, to facilitate the analysis, the proposed DMR precooling process (shown in Fig. 3) will be investigated and compared with the reference SMR (shown in Fig. 2) and their liquefaction part is assumed to be identical with the reference study [33]. Both the reference and the proposed processes are developed for large-scale hydrogen liquefaction with hydrogen feed flow of 300 TPD. At the design point conditions of the reference SMR process (Fig. 2), the mixed refrigerant is compressed in mixed refrigerant compressor (MRC 1) from 2 bar to 7 bar (process 5–6), cooled down to a temperature of 25 °C (6–7) by cooler 1 (CL1), and separated to vapor-phase mixture and liquid-phase mixture in separator 1 (S1). The vapor-phase mixture is compressed to 16 bar by MRC2 (8–8′) and cooled through CL2 to 25 °C (8′-9).The liquid-phase mixture is pumped to 16 bar (10–11). The pressurized mixtures are mixed in mixer 3 (M3) and separated again in S2. Then, the new vapor-phase mixture (state 13) is passed through the first heat exchanger (HX1, 13–14) and separated again in S3. The final vapor-phase mixture (state 15) is passed
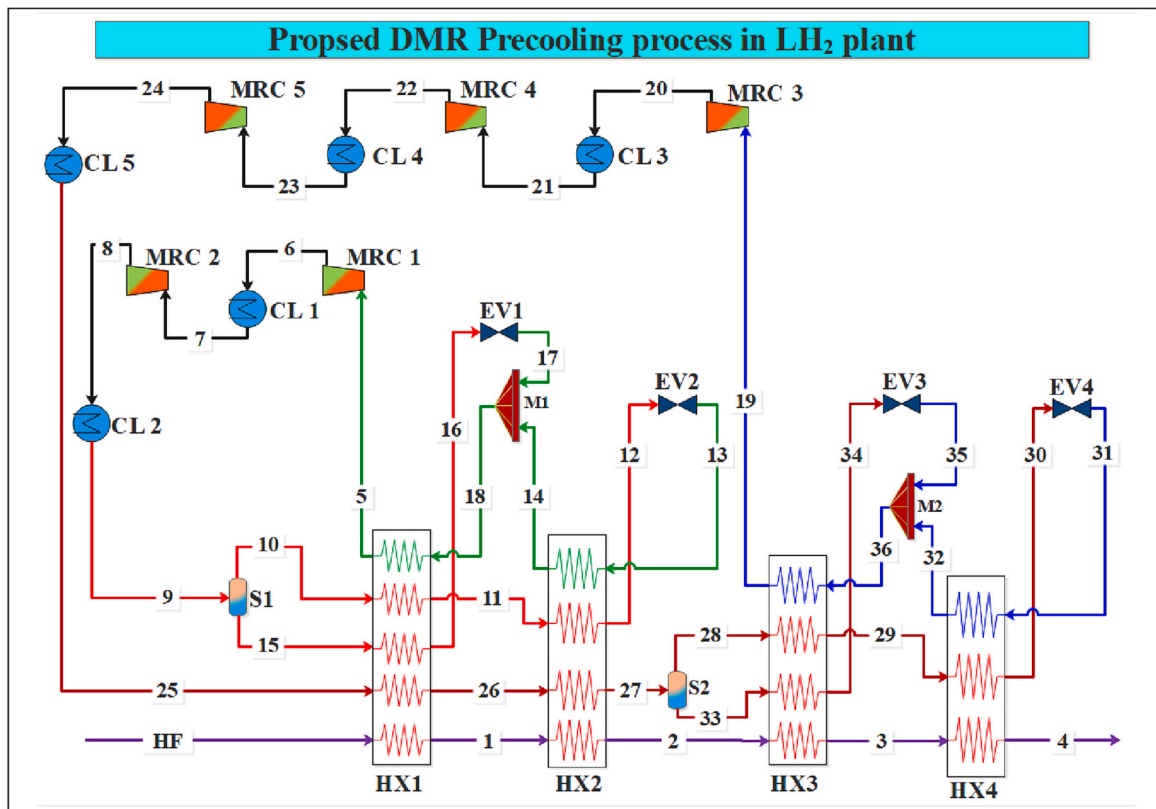

Fig. 3. Flowsheet of the proposed DSMR precooling process in LH2 plant.

through HX2 and HX3, expands though expander 3 (Exp.3) to a pressure of 2 bar, and performs evaporation process (cold duty of HX3) through the process 18–19. Similarly, the final liquid mixture (at state 20) passes through HX2 (20−21), expands through Exp.2 (21−22), and mixes with stream 19 in M2 to perform the evaporation process of HX2 (23−24). The liquid-phase mixture at state 25 passes through HX1 (25−26), expands through Exp.1 (26−27), and mixes with stream 25 in M1 to perform the evaporation process of HX1 and then the whole mixture is directed back to the inlet of MRC1 (28−5).

As mentioned earlier, in the proposed DMR process (Fig. 3), two mixed refrigerants are used to perform the precooling process. Each mixed refrigerant is circulated in a separate loop such that the first mixed refrigerant (MR1) provides the cold duty of HX1 and HX2, while the second refrigerant mixture (MR2) provides the cold duty of HX3 and HX4. At the design point conditions of the proposed process, the MR1 is compressed from 3.1 bar to 11.9 bar through two-stage intercooled compression process (5–9) using MRC1, CL1, MRC2, and CL2. At state 9, the MR1 is separated into vapor-phase mixture (10) and liquid-phase mixture (15). The mixture at stream 10 is passed through HX1 (10−11) and HX2 (11−12) to expand through expansion valve (EV2, 12–13) and perform the evaporation process of HX2 (13–14). Also, the mixture at stream 15 is passed through HX1 (15–16), expands in EV1 (16–17), and mixed with stream 14 in M1 to perform the evaporation process of HX1 and then directed back to the inlet of MRC1 (18–5). Similarly, the MR2 is compressed from 4.7 bar to 39.0 bar through three-stage intercooled compression process (19–25). Then, the MR2 enters HX1 at 21 °C and cooled down to a temperature of -23 °C through HX1 (25–26) and to a temperature of -53 °C through HX2 (26–27). Then, the MR2 is separated into vapor-phase mixture (28) and liquid-phase mixture (33) by S2. The vapor-mixture (28) is passed through HX3 (28–29) and HX4 (29–30) to expand through EV4 (30−31) and perform the evaporation process of HX4 (31−32). Also, the liquid-mixture (33) is passed through HX3 (33–34), expands in EV3 (34–35), and mixed with stream 32 in M2 to perform the evaporation process of HX3 and directed back to the inlet of MRC3 (36−19).

The use of expansion valves rather than expanders for the throttling process in the present DMR process aims to avoid using moving parts (the expanders) at cryogenic temperatures resulting in high reliable system and easy to scale-up. This is another important advantage of the proposed DMR process.

3. Methodology

The proposed DMR process and the reference SMR process are analyzed using energetic, exergetic, environmental, and economical models, which are presented in this section.

3.1. Energy analysis

The energetic performance of the precooling SMR and DMR processes is simulated using Aspen HYSYS and then thoroughly analyzed and evaluated. Calculations were performed to compare the results using Soave-Redlich-Kwong (SRK) vs. Peng-Robinson equation of state (EOS). The results show that both equations have mostly the same results with relative difference less than 0.1 %. If ortho-para converters are included, which are used within or after the liquefaction part of the hydrogen liquefaction plant, then the MBWR EOS is preferred over Peng-Robinson EOS for the hydrogen streams as recommended by Azizbadi et al. [41]. As the precooling process in this study does not include ortho-para converter, Peng-Robinson EOS can be used for both hydrogen and mixed refrigerant properties. In addition, this equation of state function is widely used in the modeling of the hydrogen liquefaction process as it has good accuracy over a wide range of pressures and temperatures as reported in [24,33,38,42]. Thus, in this study, Peng-Robinson equation of state is implemented to calculate the thermodynamic properties of all streams. For the thermodynamic analyses of

these processes, the following assumptions are made:

- Steady-state conditions.
- The impurities in the hydrogen have been removed before the precooling process as the impurities usually removed in the hydrogen production stage [42]. Therefore, the expenses associated with impurity removal have not been considered in the economic analysis of this study.
- The pressure drops through the coolers and heat exchangers are negligible [33,38,42,43].
- The hydrogen gas is fed to the process at temperature of 25 °C, pressure of 21.0 bar, and precooled to −192 °C. This level of temperature is recommended for the hydrogen precooling process before directing it to the ortho-para converters through the liquefaction process [20].
- For the proposed DMR process, the minimum internal temperature difference of the heat exchangers does not exceed 0.50 °C to ensure efficient performance of the cryogenic heat exchangers [44].

Energetic analysis provides critical information that can be used to optimize the performance of a process, reduce costs, and minimize its environmental impact. Therefore, in this study, the energetic performance of the SMR and DMR precooling processes was compared using two performance indicators: the specific energy consumption (SEC) and the coefficient of performance (COP). The comparison was based on the total compression power and the total cold duty of their heat exchangers, with the mixed refrigerant compositions presented in Table 4. The goal of this comparison is to identify the more efficient and cost-effective hydrogen precooling process. The SEC is calculated by dividing the net total compression power of the precooling process by the mass flow rate of the hydrogen feed as:

$$SEC = \frac{\sum \dot{W}_{MRC,i} - \sum \dot{W}_{Exp,i}}{\dot{m}_{HF}} \tag{1}$$

where $\sum \dot{W}_{MRC,i}$ is the total compression power of all mixed refrigerant compressors, $\sum \dot{W}_{Exp,i}$ is the total power generated by the liquid expanders (applicable only for the reference SMR process [33]), and $\dot{m}_{HF}$ is the flow rate of the hydrogen feed stream. The COP is defined as:

$$COP = \frac{\sum Q_{HX,CD}}{\sum \dot{W}_{MRC,i} - \sum \dot{W}_{Exp,i}} \tag{2}$$

where $\sum Q_{HX,CD}$ is the total cold duty of all heat exchangers. After the simulation process is conducted in ASPEN HYSYS, the data of all streams and equipment (including pressure, temperature, and flow rate of each stream (see supplementary material Table S.1), the cooling duty of each HX and cooler (Table 5), and the compression power of each compressor (Table 5)) are exported to Excel files to perform the exergetic, and economic analyses of the processes as described below in Section 3.2, and Section 3.3, respectively. The results of the energy analysis at the design conditions of the SMR process and the DMR process are presented, compared, and discussed in Section 4.1. The design specification of the present hydrogen precooling process are shown in Table 1.

Table 1
Design specification of the proposed hydrogen precooling process.

Parameter	Value (range)
Hydrogen feed temperature, [°C]	25
Hydrogen feed pressure, [bar]	21
Hydrogen feed flow rate, [kg/s]	3.45 (1.16–11.6)
Aftercooler temperature, [°C]	21
Design precooling temperature (T_4), [°C]	-192 °C
Precooling pressure (P_4), [bar]	21
Isentropic efficiency of compressors, (%)	90
Pressure drop across heat exchangers and aftercoolers, [bar]	0

3.2. Exergy analysis

Exergy analyses of the proposed precooling process in this study are performed to identify and locate the sources of the thermodynamic inefficiency. Based on that, the design of these equipment can be further improved to minimize the exergy destruction which yields minimum power consumption in the present refrigeration systems. The total exergy at each stream on the process ($\dot{E}_{tot}$) is defined as the summation of the physical exergy ($\dot{E}_{ph}$) and chemical exergy as ($\dot{E}_{ch}$) [45]:

$$\dot{E}_{tot} = \dot{E}_{ph} + \dot{E}_{ch} \tag{3}$$

where the physical exergy is defined as:

$$\dot{E}_{ph} = \dot{m}_i[(h_i - h_o) - T_o(s_i - s_o)] \tag{4}$$

where h_o and s_o refer to the enthalpy and entropy of the flow at the ambient temperature and pressure (dead state), which is obtained from Aspen HYSYS library at temperature of 298.15 K and pressure of 1.013 bar. And h_i, s_i, and $\dot{m}_i$ refer to the enthalpy, entropy, and mass flow rate of each flow stream as presented in supplementary material Table S.1. The chemical exergy is defined as [33]:

$$\dot{E}_{ch} = \sum \left(x_j \dot{E}_j^o \right) + \dot{G} - \sum \left\{ x_j \dot{G}_i \right\} \tag{5}$$

where x_j, $\dot{E}_j^o$, and $\dot{G}$ stand for the mole fraction of component j, standard chemical exergy of component j, and the Gibbs free energy rate, respectively. The values of $\dot{E}_j^o$ are obtained from [46]. Also, the Gibbs free energy rate is calculated by the method developed in [33]. The definitions of the exergy irreversibility and exergy efficiency of the precooling process equipment are presented in Table 2.

Also, overall exergy efficiency of the precooling process is defined as:

$$\varepsilon_{overall} = \left\{ \dot{E}_{Product} - \dot{E}_{Feed} \right\} \Big/ \dot{W}_{total} \tag{6}$$

The exergy analysis results are presented and discussed in Section 4.2.

3.3. Economic analysis

The economic evaluation of the reference SMR process was not performed by its authors in [33]. Therefore, in this study, the module costing techniques (Guthrie's method) is adapted and performed for the economic evaluation of both SMR and DMR precooling processes. This method is used to determine the cost of a process by breaking it down into smaller modules or components. The cost of each module is then determined, and these costs are added together to arrive at the total cost of the process. In particular, this method useful when the process is complex and made up of many different parts or components. Therefore, it is typically used to estimate the costs of new chemical plants. The equipment purchase cost (E_p) is obtained from [11]:

$$log_{10}\left(E_{p,k}\right) = K_1 + K_2 \times log_{10}(A) + K_3 \times \left(log_{10}(A)\right)^2 \tag{7}$$

where A is the capacity parameter of the equipment, K_1, K_2, and K_3 are the cost constants (their values for each equipment are presented in the supplementary material in Table S.3 and Table S.4). Once E_p is obtained, the cost of the base module is calculated as:

$$C_{BM,k} = E_{p,k} \times F_{BM,k} \tag{8}$$

where F_{BM} is the module cost factor (assumed to be 1.0 in this study, as the operating pressures and temperatures are within the applicable range for the original formula shown in Eq. (8)). The operational cost of each process is calculated at an electricity cost of 0.06 \$/kWh (526 \$/kW-yr) [11] as:

$$OC = electricity\ cost\ \left(\$/kW \bullet yr\right) \times \left(\sum \dot{W}_{MRC,i} - \sum \dot{W}_{Exp,i} \right)(kW) \tag{9}$$

To compare the economic costs of the SMR process and the DMR process, three economic indicators are used, which are: the total capital investment (TCI), grass root cost (GRC), and the total annualized cost (TAC) defined as:

$$TCI = 1.18 \times \sum_{k}^{m} C_{BM,k} \tag{10}$$

$$GRC = TCI + 0.5 \times \sum_{k}^{m} C_{BM,k} \tag{11}$$

$$TAC = \frac{TCI}{PBP} + OC \tag{12}$$

where PBP is the payback period and is set to five years. The results of the economic analysis are presented and discussed in Section 4.3.

3.4. Validation

To verify the accuracy of the simulation process in this study, the energetic performance of the reference SMR process was performed and compared with the results reported in [33] as shown in Table 3 under the same design conditions. This approach is performed to appraise the accuracy of the simulation process ad demonstrated by Saedi et al. [48]. The results of the simulation process are identical with those reported in with an absolute relative error of less than 0.37 %.

4. Results and discussion

This section discusses the energetic, exergetic, economic, and environmental performances of the proposed DMR hydrogen precooling process and compares them to that of the reference SMR precooling process (Section 4.1 to 4.4). Also, further comparison with other

Table 2
Definitions of the exergy irreversibility and efficiency of the precooling process equipment [23,26,47].

Equipment	Exergy irreversibility	Exergy efficiency
Heat exchangers/ coolers	$\dot{I} = \sum_1^n \left(\dot{E}_i\right)_{in} - \sum_1^n \left(\dot{E}_i\right)_{out}$	$\varepsilon_{HX} = \sum_1^n \left(\dot{E}_i\right)_{out} \Big/ \sum_1^n \left(\dot{E}_i\right)_{in}$
Compressors	$\dot{I} = \dot{E}_{in} - \dot{E}_{out} - \dot{W}_{MRC}$	$\varepsilon_{MRC} = 1 - \dfrac{\dot{I}}{\dot{W}_{MRC}}$
Mixers	$\dot{I} = \sum_1^n \left(\dot{E}_i\right)_{in} - \dot{E}_{out}$	$\varepsilon_{MRC} = 1 - \dfrac{\dot{I}}{\sum_1^n \left(\dot{E}_i\right)_{in}}$
Separators	$\dot{I} = \dot{E}_{in} - \sum_1^n \left(\dot{E}_i\right)_{out}$	$\varepsilon_S = \dfrac{\sum_1^n \left(\dot{E}_i\right)_{out}}{\dot{E}_{in}}$
Expansion valves	$\dot{I} = \dot{E}_{in} - \dot{E}_{out}$	$\varepsilon_S = \dfrac{\dot{E}_{out}}{\dot{E}_{in}}$

Table 3
Validation of the simulation process compared to the results reported in [33].

Parameter	SMR process in this study	SMR process in [33].	ARE, (%)
Total cold duty, [kW]	54.35	54.40	0.01
Total compression power, [kW]	13.44	13.49	0.37
Precooling temperature, [°C]	-193	-193	0.00

ARE, (%) = 100 × | SMR process in this study - SMR process in [33]/ SMR process in [33].

precooling processes is conducted in these sections based on the available data in the literature. Furthermore, the sensitivity analysis of the proposed DMR process is introduced in Section 4.5.

4.1. Energetic performance

From the configuration of the DMR shown in Fig. 3, it can be noted that the first two heat exchangers (HX1 and HX2) have higher cooling duty than of HX3 and HX4. This is because that HX1 and HX2 are responsible to: (1) cool the hydrogen stream from 25 °C to -53 °C, (2) cool the MR2 stream from 21 °C to -53 °C, (3) cool the liquid stream of MR1 from 21 °C to -23 °C, and (4) cool the vapor stream of MR1 from 21 °C to -53 °C. While the other two heat exchangers (HX3 and HX4) are responsible to: (1) cool the hydrogen stream from -53 °C to -192 °C, (2) cool the liquid stream of MR2 from -53 °C to -140 °C, and (3) cool the vapor stream of MR2 -53 °C to -192 °C. Notice that because the loads of HX1 and HX2 are higher than HX3 and HX4, the composition of the MR1 should be consisted of heavy refrigerants (such as propane, n-pentane, ammonia, etc.) to match higher cooling loads at low desired temperature. In contrast, the composition of MR2 should be consisted of light refrigerant (such as methane, nitrogen, ethylene, etc.) to provide the extremely low temperatures required in HX3 and HX4. The flowchart of the applied steps to determine the composition of MR1 and MR2 is presented in the supplementary material (Fig. S.1). Following these steps, after several iterations, the final composition of MR1 and MR2 is presented in Table 4. It is worth mentioning that the values of the optimum temperatures above were reached via a rigorous iterative process by observing and correcting the composite curves of all heat exchangers.

As shown in Table 4, compared to the mixed refrigerant composition of the reference SMR process, the composition of MR1 contains significant part of ammonia (28 %), which is also contained in the composition of MR2 as a minor refrigerant (4.21 %). The existence of ammonia in MR1 and MR2 improves the heat flow rate per unit mass in HX1 and HX3, which reduces the total required flow rates and thus the compression power is reduced. In addition, both MR1 and MR2 contain zero fractions of hydrogen, R-14, and n-Butane. It is noted that these components increase the compression power without significant improvement in the composite curves of the heat exchangers; therefore, they are removed from the composition of MR1 and MR2.

The composite curves of the heat exchangers obtained with MR1 and MR2 are presented in Fig. 4. It is noted that these mixtures exhibit extraordinary efficient performance as the temperature difference between the hot and cold composite curves does not exceed 5 °C as in HX1 (compared to 12 °C in reference case) and approaches zero as in HX3 (compared to 1 °C in reference case). Therefore, the energy performance of the proposed DMR is significantly improved compared to the reference SMR process as explained in the next paragraph.

To compare the energetic performance of the proposed and the reference precooling processes, the hydrogen inlet and outlet conditions,

the isentropic efficiency of the compressors, and the outlet temperatures from the coolers are set the same. The obtained results are summarized in Table 5. It is noted that the total flow rate of the MR1 and MR2 (80 kg/s) is less than the flow rate in the SMR process (98 kg/s). In addition, as the cold duty of HX1 (18.71 MW) and HX2 (9.16 MW) are larger than of HX3 (14.44 MW) and HX4 (5.11 MW), MR1 has higher flow rate (47 kg/s) than of MR2 (33 kg/s), However, because MR1 is compressed to 11.90 bar which is lower than of the MR2 (39.00 bar) and the components of MR1 are heavier than of MR2, the compression power of MR1 (4.01 MW) is 40 % less than of MR2 (6.69 MW) in the proposed DMR process. This implies that the proposed DMR process provides flexibility in the distribution of quantity (amount of heat absorbed) and quality (level of temperature) of the cold duty through the heat exchangers, which is not feasible by using SMR process. This means that the operation of the DMR process is more efficient than of the SMR process. From energy point of view, this was proved by comparing the specific energy consumption (SEC) and the coefficient of performance (COP) of both processes, as shown in Table 5. It is found that the SEC of the DMR process (0.862 kWh/kgH$_{2Feed}$) is less than of the reference SMR process (1.082 kWh/kgH$_{2Feed}$) by 20.33 %. At hydrogen flow rate of 3.45 kg/s, the total compression power is reduced from 13.44 MW in the SMR process to 10.70 MW in the DMR process. Also, the total cold duty of the heat exchangers is reduced from 52.06 MW (in SMR) to 47.42 MW (in DMR). Therefore, the COP of the DMR process (4.43) is higher than of the SMR process (3.87) by 14.47 %. As the total cold duty and total compression power of the DMR are significantly less than of the SMR, this will minimize the capital and operational costs of the DMR process as discussed in Section 4.3.

The SEC of 0.862 kWh/kgH$_{2Feed}$ is obtained with a minimum internal temperature difference (MITD) of 0.17 °C in HX1, 0.19 °C in HX2, 0.04 °C in HX3, and 0.10 °C in HX4. To obtain higher MITD, to ensure the design feasibility of these heat exchangers, the mass flow rates of MR1 and MR2 have to be increased. For instance, if the flow rate of MR1 is increased from 47 kg/s to 52 kg/s, and of MR2 from 33 kg/s to 35 kg/s, the MITD will be 1.96 °C in HX1, 0.93 °C in HX2, 1.38 °C in HX3, and 0.11 °C in HX4. At these conditions, the SEC is 0.903 kWh/kgH$_{2Feed}$, which is 4.7 % higher than at the lower flow rates of MR1 and MR2 (0.862 kWh/kgH$_{2Feed}$). However, this SEC is still 16.5 % lower than of the reference SMR process.

Despite the efficient performance of the proposed DMR compared to the reference SMR process, it is worth to compare its capacity and SEC with other hydrogen precooling processes available in the literature as shown in Table 6. It is found that the developed in this study DMR process is superior even when compared to the best performing SMR of the reference [33] followed by the SMR process introduced by Ghorbani et al. [24]. Also, there are huge differences between the SEC of the present DMR process and of that used CO$_2$ as a pure refrigerant in [11] or the SMR presented in [13] by 63.63 %, and 57.97 %, respectively. In addition, the precooling target temperature of the process in [11] is -160 °C compared to lower than -190 °C of the other listed processes. This implies that the mixed refrigerant processes have superior performance compared to pure refrigerant processes. Although the process in [13] is a SMR process and its hydrogen flow rate is only 1.00 kg/s (70 % lower than in the present study), the selected components of its refrigerant mixture contain R-14, Neon, and n-Butane which form 20 % of the mixture compositions. These refrigerants, as noted during the development of the new proposed refrigerants in this study, increase the compression power with a slight improvement in the heat exchanger performance.

The main findings of this section is that: (a) from energy point of view, the DMR hydrogen precooling process is more efficient than of the pure-refrigerant and SMR process; (b) The proposed DMR reduces the SEC by 20.33 % and improves the COP by 14.47 % compared to the most competitive SMR process in [33].
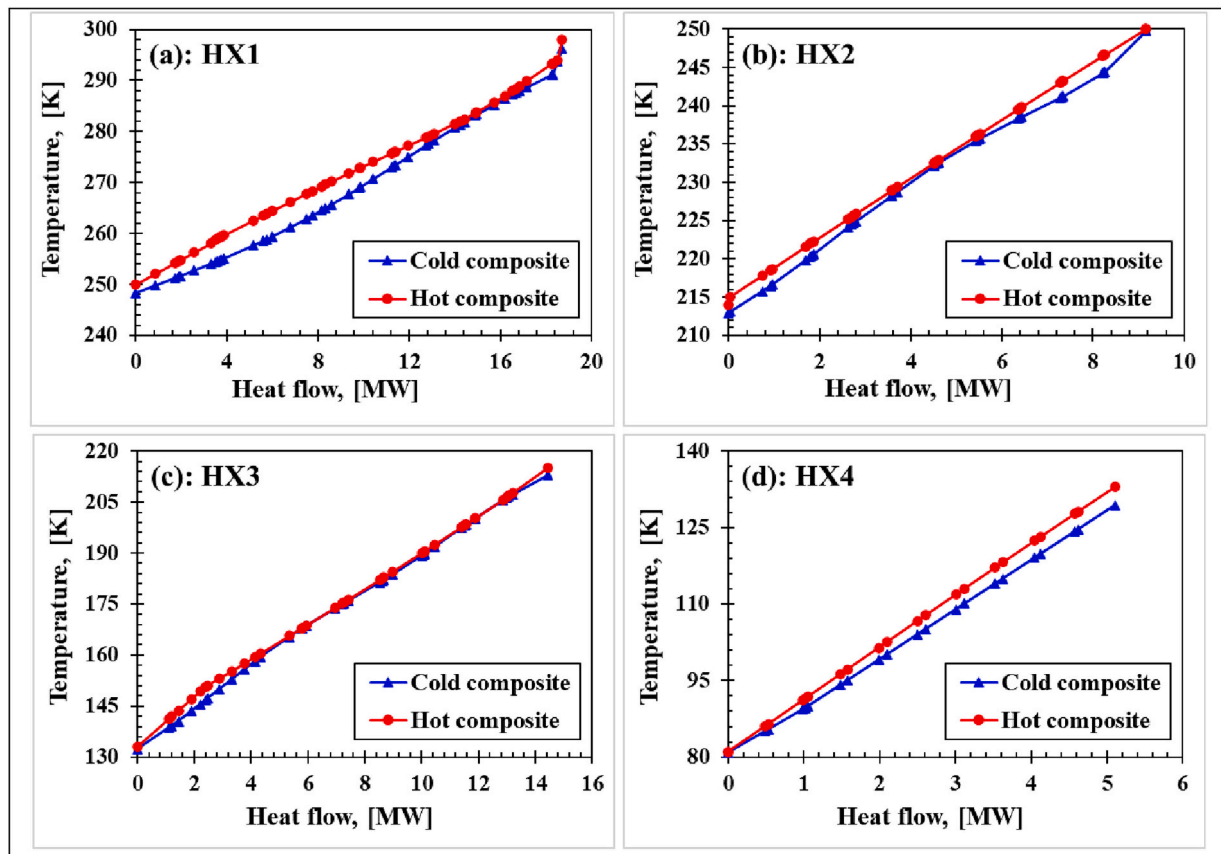
Table 4
Chemical composition (Molar-basis) of the mixed refrigerant of the reference SMR and proposed DMR precooling processes.

Components	Reference SMR, [%]	Proposed DMR	
		MR1, [%]	MR2, [%]
Methane	17.00	0.000	38.03
Ethane	7.000	10.00	0.000
Propane	18.00	28.00	5.700
n-Butane	2.000	0.000	0.000
i-Pentane	0.000	14.50	0.000
n-Pentane	15.00	4.000	0.000
Nitrogen	16.00	0.000	23.06
Hydrogen	1.000	0.000	0.000
Ethylene	16.00	15.50	29.00
R-14	8.000	0.000	0.000
Ammonia	0.000	28.00	4.210

Fig. 4. Composite curves of (a) HX1, (b) HX2, (c) HX3, and (d) HX4.

Table 5
Comparison of the performance indicators between the proposed DMR process and reference SMR process identical design conditions.

Item	Reference SMR process	Proposed DMR process
Configuration	Single MR loop	Dual MR loops
Precooling range	From 25 °C to −192 °C	From 25 °C to −192 °C
Adiabatic eff. of the compressors, [%]	90	90
Hydrogen flow rate (feed), [kg/s]	3.45	3.45
Outlet temperature from the cooler, [K]	294	294
Exchanger cold duty, [MW]	52.06	47.42
Compression power, [MW]	13.44	10.70
MR flow rate, [kg/s]	98.00	47.00 (MR1), 33.00 (MR2)
MR low-pressure, [bar]	2.00	3.10 (MR1), 4.70 (MR2)
MR high-pressure, [bar]	16.00	11.90 (MR1), 39.00 (MR2)
COP of precooling process	3.87	4.43
Total coolers' load, [MW]	23.82	21.41
SEC, [kWh/kgH$_{2Feed}$]	1.082	0.862

4.2. Exergetic performance

The tabulated results of the exergy analysis of the present DMR precooling process are given in the supplementary material (Table S.2). The analysis revealed that the overall exergy efficiency is 68.02 %. As shown in Fig. 5, the heat exchangers of the process are responsible for about 33 % of the exergy irreversibilities followed by coolers with 31 %. This implies that further improvement for the process performance can be achieved by optimizing the heat exchanger design and the cooling

conditions of the coolers. The contribution of separators and mixers to the total exergy destruction is mostly negligible and did not present in Fig. 5. The exergetic performance of the proposed DMR (68.02 %) is close to that of the reference SMR (

67.53 %). Although the exergetic performance of the present process can be improved by replacing the expansion valves with expanders (as performed in the reference process), using expansion valves ensures operating reliability and minimize the initial and operational costs of the process. The high exergy efficiency of the precooling process is much higher than of the liquefaction process (52.24 %) as the liquefaction process is conducted at extremely low temperature with lighter refrigerants. However, enhancing the exergy efficiency of the DMR precooling cycle could enhance the exergy efficiency of the overall liquefaction process which will be further investigated in future work.

4.3. Economic analysis

The economic evaluation of the present DMR process and the reference SMR process is conducted in terms of the total capital investment (TCI), grass root cost (GRC), and the total annualized cost (TAC) and presented in Fig. 6. These costs are calculated based on Eqs. (7) to (12). The equipment purchase cost (E_p) is obtained from Ref. [11]. The breakdown of the equipment costs is presented in the supplementary material (Table S.3 for the SMR, and Table S.4 for the DMR). The capital cost of the miscellaneous components (mixers, separators, and control valves excluding the expanders that were considered as major components) is calculated by the authors for several similar cycles and found to be about 1.00 % of the total costs of the other components in the SMR process. For the proposed DMR process, a conservative 2.00 % is used, which accounts for the control valves that replaced the liquid expanders used in SMR and accounts for the expansion valves. Furthermore, the payback period was set to five years and the plant maintenance cost is

Table 6
Comparison between the proposed DMR process and other processes (available in the literature) used for hydrogen precooling.

Reference	Configuration	Feed hydrogen conditions			T_4, [°C]	SEC, [kWh/kgH$_{2Feed}$]	Reduction percent[a], [%]
		T, [°C]	P, [bar]	$\dot{m}$, [kg/s]			
[33]	SMR	25	21	3.450	-192	1.082	20.33
[11]	CO$_2$-precooled	25	21	1.157	−160	2.370	63.63
[13]	SMR	37	21	1.000	−198	2.051	57.97
[24]	SMR	27	21	0.620	−195	1.113	22.55
[22]	SMR	25	21	1.157	−198	1.416	39.12
Present study	DMR	25	21	3.450	−192	0.862	–

[a] Reduction percent is calculated relative to the SEC of the present study as: Reduction percent [%] = 100 ×(SEC of reference study -SEC of present study)/SEC of reference study.
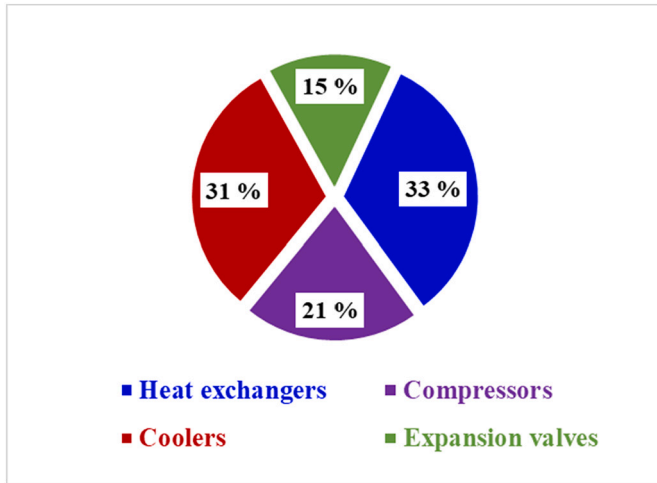

Fig. 5. Contribution of the DMR process equipment in the total exergy destruction of the process.
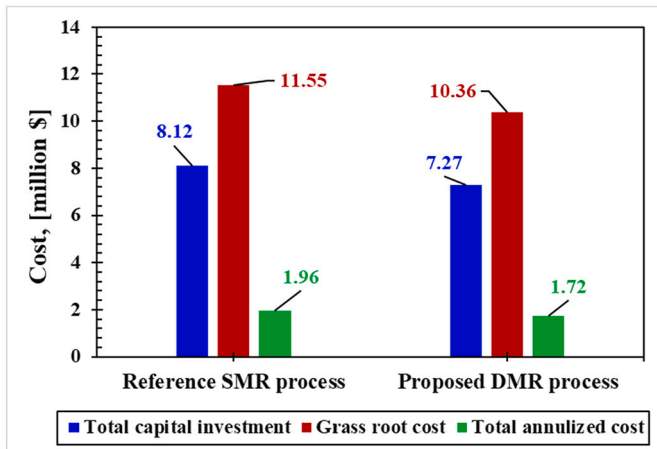

Fig. 6. Comparison between the proposed DMR process and the reference SMR process in terms of the total capital investment, grass root cost, and total annualized cost.

fixed at 2.00 % of the TCI. From Fig. 6, it is found that the TCI, GRC, and TAC of the present DMR process are lower than of the reference SMR process by 10.46 %, 10.30 %, and 12.24 %, respectively. The reduction on these costs achieved by the DMR process can be explained by the following reasons: (1) the total cold duty of the heat exchangers in the DMR process (47.42 MW) is reduced by 8.91 % compared to the SMR process (52.06 MW), which reduces the capital costs of the heat exchangers; (2) as the total flow rate of MR1 and MR2 in the DMR process (80 kg/s) is lower than in the SMR process (98 kg/s), the total coolers'

load is reduced by 10.11 % (from 23.82 MW in SMR to 21.41 in DMR), which reduces the capital cost of the coolers; (3) the DMR process utilizes control valves for the expansion process rather than the more expensive liquid expander which further reduces the TCI; and (4) the compression power in the DMR (10.70 MW) is less than in the SMR (13.44 MW) by 20.40 %, which significantly reduces the operational cost of the DMR process (from 0.34 million $/year in the SMR to 0.27 million $/year in the DMR process).

4.4. Environmental analysis

Although the production of liquid hydrogen is considered as a promised solution to reduce the CO_2 emission, its production, liquefaction, and transportation using fossil-fuel-based electricity will not lead to significant benefits from environmental point of view. To make the hydrogen as eco-friendly fuel, its generation and liquefaction should be driven using renewable energy resources. However, as the renewable sources suffer from several issues such as limited abundancy, fluctuations, and high capital investment, the utilization of the fossil-fuel-based energy seems to be unavoidable. Thus, minimizing the SEC of the generation and liquefaction processes is essential to reduce their CO_2 emissions. In this section, assuming the precooling process is driven using fossil-fuel-based energy (electricity), the CO_2 emissions of the present DMR process is compared with other pure-refrigerant and SMR precooling process as shown in Fig. 7. The amount of CO_2 emissions is calculated as:

$$CO_2 emission \left[\frac{tons}{year}\right] = SEC \left[\frac{kWh}{kgH_2}\right] \times \dot{m}_{FH}\left[\frac{kg}{h}\right] \times CO_2 emissions \left[\frac{tons}{kWh}\right] \times 8760 \left[\frac{h}{year}\right]$$

(13)

where the SEC of each process is taken from Table 6, and the feed hydrogen flow is 12.5 kg/h which is equivalent for 300 TPD. As the amount of CO_2 emissions is calculated in tons per year basis assuming the electricity is provided from natural gas power plant, CO_2 emission amount of 0.0000411 tons/kWhe [49] is used. From Fig. 7, it is found that the DMR process proposed in the present study reduces the CO_2 emissions by 20.33 % to 63.63 % compared to all other five technologies.

4.5. Sensitivity analysis

In Section 4.5.1, the sensitivity of the present DMR process is analyzed against five operating parameters including the flow rate of the feed hydrogen ($\dot{m}_{HF}$), the high-pressure of MR1 ($P_{h,MR1}$), the high-pressure of MR2 ($P_{h,MR2}$), the low-pressure of MR1 ($P_{l,MR1}$), and the low-pressure of MR2 ($P_{l,MR2}$). The sensitivity of the DMR process is evaluated using three performance indicators: compression power, SEC, and COP. During the analysis of the five mentioned parameters, only one parameter is changed, and the other parameters kept fixed at the design point conditions (presented in Table 4) except the flow rates of MR1 and
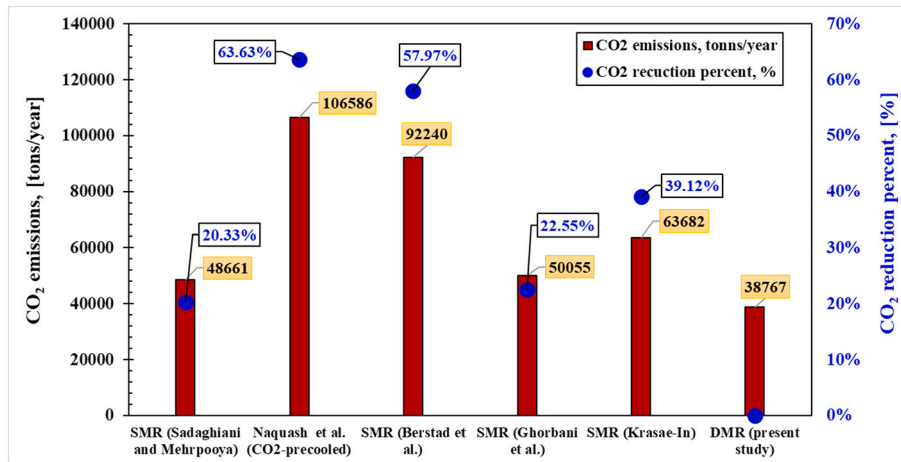
Fig. 7. Comparison of CO2 emissions if the present DMR and other pure refrigerant and SMR processes are driven by fossil-fuel-based electricity. The solid circle symbol represents CO2 reduction of the proposed DMR compared to all other 5 processes.

MR2. For each simulated parameters, the flow rates of MR1 and MR2 are adjusted until the composite curves of the heat exchangers match those obtained at the design conditions. Then, in Section 4.5.2, the effects of the mixed refrigerant composition on the performance of the proposed process are discussed.

4.5.1. Effects of operating parameters

Fig. 8 shows the relationship between the $\dot{m}_{HF}$ and the performance indicators of the present DMR process. It is found that the flow rates of MR1 ($\dot{m}_{MR1}$), MR2 ($\dot{m}_{MR2}$), and the compression power linearly increase as $\dot{m}_{HF}$ increases from 1.16 kg/s (100 TPD) to 11.57 kg/s (1000 TPD). In addition, the slope of $\dot{m}_{MR1}$ curve is higher than of $\dot{m}_{MR2}$ curve which minimizes the compression power as the high-pressure of MR1 (11.9 bar) is lower than of MR2 (39.0 bar). Furthermore, over the range of $\dot{m}_{HF}$, the SEC and COP are slightly changing around 0.863 kWh/kgH$_{2Feed}$ and 4.43, respectively. A maximum SEC of 0.865 kWh/kgH$_{2Feed}$ is noted at $\dot{m}_{HF}$ of 1.74 kg/s (150 TPD) and a minimum SEC of 0.860 is noted at $\dot{m}_{HF}$ of 8.10 kg/s (700 TPD), which is only 0.58 % lower than the maximum one. This proves that the composition of the new mixtures

(MR1 and MR2) can handle different capacities without losing the efficient performance on the heat exchanger and enjoy semi-constant SEC and COP.

Unlike the effect of $\dot{m}_{HF}$, the high-pressures of MR1 ($P_{h,MR1}$) and MR2 ($P_{h,MR2}$) have significant effects on the performance of the DMR process as shown in Fig. 9(a), and Fig. 9(b), respectively. From Fig. 9(a), it can be noted that changing the $P_{h,MR1}$ does not affect the flow rate of MR2 as the temperature set of the heat exchangers does not change; thus $\dot{m}_{MR2}$ kept constant. As $P_{h,MR1}$ increases from 8.0 to 16.0 bar, the SEC first decreases from 0.944 kWh/kgH$_{2Feed}$ (at 8.0 bar) to a minimum value of 0.866 kWh/kgH$_{2Feed}$ (at 12.0 bar) then increases up to a maximum value of 1.482 kWh/kgH$_{2Feed}$ (at 16.0 bar). In contrast, as shown in Fig. 9(b), the increase of $P_{h,MR2}$ from 15.0 bar to 50.0 bar decreases both $\dot{m}_{MR1}$, and $\dot{m}_{MR2}$ which minimizes the SEC from 1.194 1.482 kWh/kgH$_{2Feed}$ (at 15.0 bar) to a minimum of 0.868 1.482 kWh/kgH$_{2Feed}$ (at 40.0 bar) and increases to 0.906 1.482 kWh/kgH$_{2Feed}$ (at 50.0 bar). However, the COP decreases over the range of $P_{h,MR1}$ and $P_{h,MR2}$. This is explained by that the increase of the high-pressures increases the specific heat of the mixtures at the hot side and decreases it in the cold side of the heat
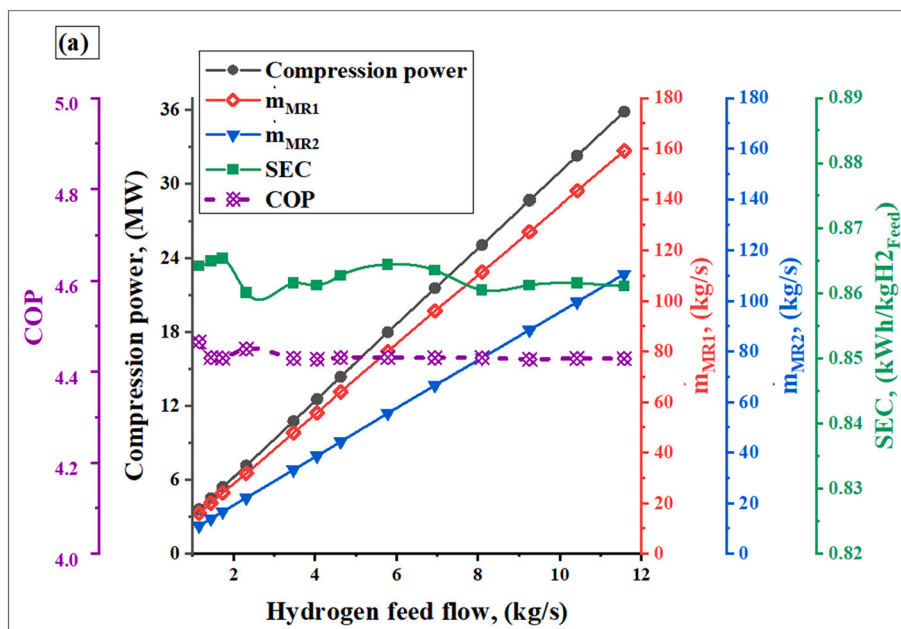

Fig. 8. Effect of the hydrogen feed flow rate on the performance indicators of the present DMR precooling process.
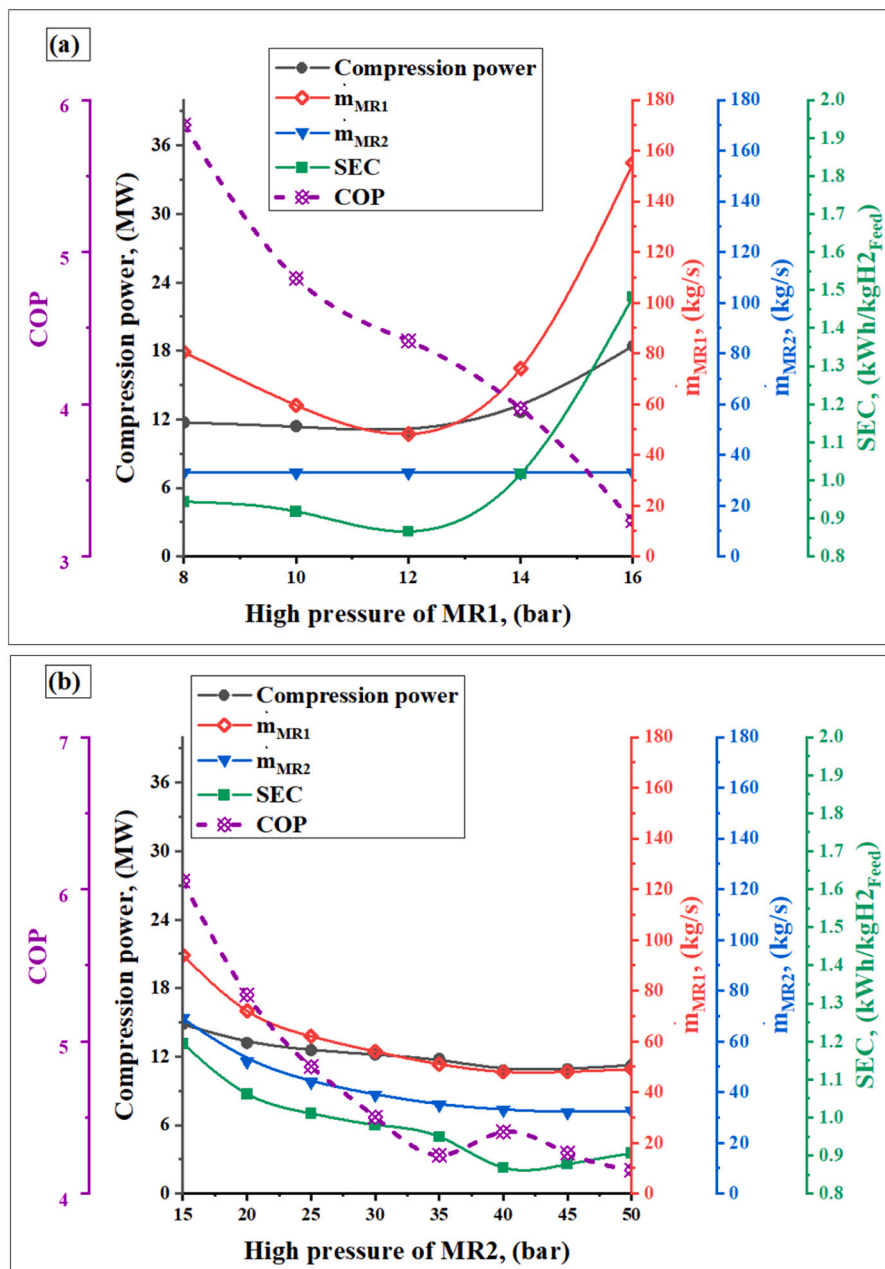
Fig. 9. Effect of the high-pressure of (a) MR1, and (b) MR2 on the performance indicators of the present DMR precooling process.

exchangers. This negatively affects the heat capacity of the heat exchanger and reduces the COP of the DMR process. Also, it is noted that at $P_{h,MR1}$ less than 12.0 bar, or $P_{h,MR2}$ less than 30.0 bar, their vapor fractions at the entrance of MRC1 and MRC2 reduce from 1.00 to 0.82 at 8.0 bar for MR1, and 0.88 at 15 bar of MR2. Therefore, higher pressures improve the quality of the mixtures at the entrance of MRC1 and MRC3 which enhance the efficiency of the compression process up to an optimum point (at which both mixtures enter the compressors at vapor fraction of 1.00). This implies that there is a trade-off between the capacity of the heat exchangers and the compression power of MRC1 and MRC2. Therefore, the high-pressure of both mixtures must be optimized to get the minimum SEC with priority for $P_{h,MR2}$ as it composed of lighter refrigerants which demand more energy for the compression process.

In contrast to the high-pressures of MR1 and MR2, the increase of their low-pressures reduces the compression power with slight changes in their flow rates up to optimum point (4.0 bar for MR1 and 5.0 bar for MR2) as shown in Fig. 10(a) and Fig. 10(b). Further increase in the low-

pressures above the optimum values requires significant increase in the flow rates of the refrigerants to avoid the temperature-cross at the cold-end of the heat exchangers, which increase the SEC above the optimum value. However, the COP increases over the full range of the low-pressures as the heat capacity of the heat exchangers increases alongside the increase of the flow rates of both refrigerant mixtures.

4.5.2. Effects of mixed refrigerants' composition

From the sensitivity analysis, it is clear that the present DMR process needs further work to optimize the SEC without reducing the COP of the process. Table 7 shows a preliminary optimization for the composition of MR1 and MR2 of the present DMR process and their operational parameters at three different capacities (Case 1: 300 TPD, Case 2: 400 TPD, and Case 3: 500 TPD). All cases have the same composition for MR1 while the composition of MR2 in Case 2 and Case 3 differs from Case 1 (by slightly increasing the fractions of the methane and ethylene with slight decrease in the nitrogen and propane fractions). The other
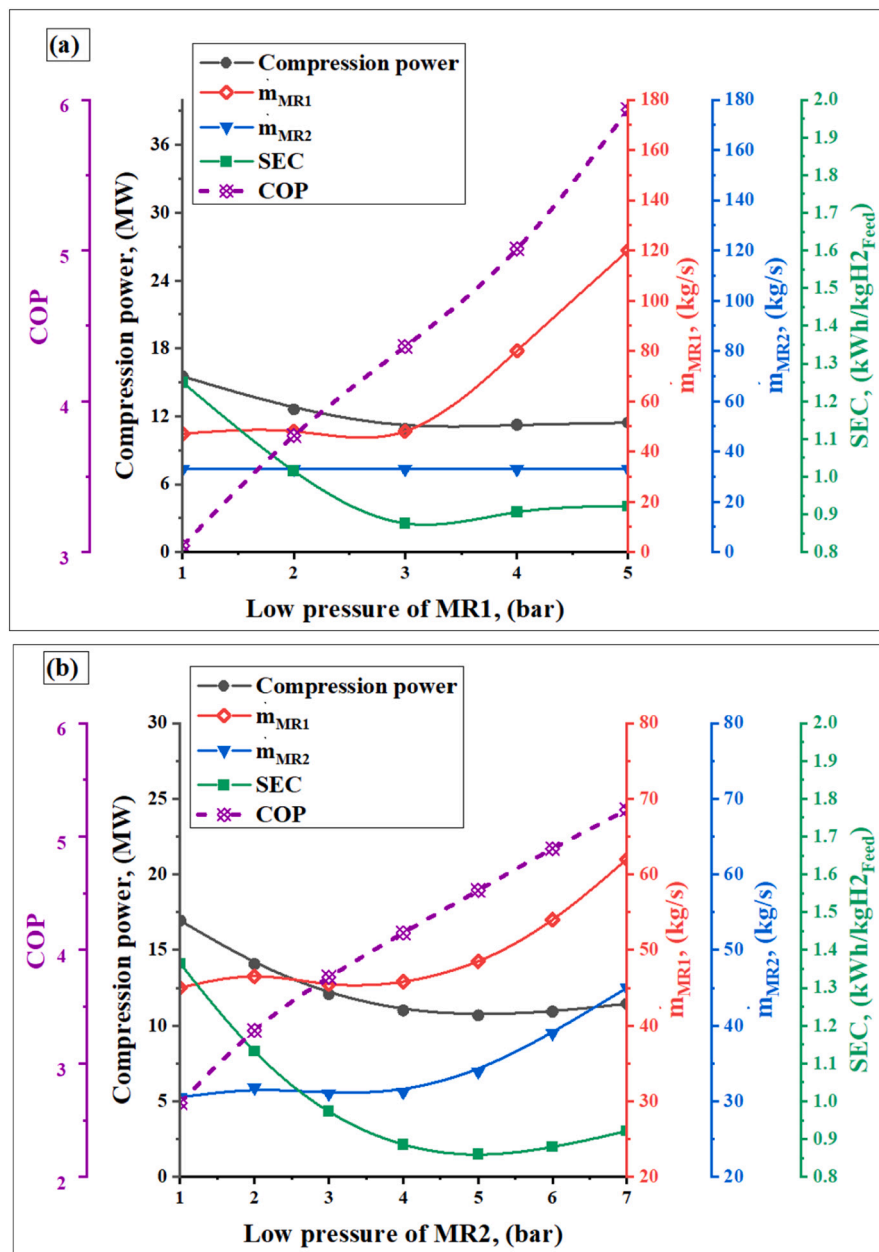
Fig. 10. Effect of the high-pressure of (a) MR1, and (b) MR2 on the performance indicators of the present DMR precooling process.

parameters were adjusted close to their optimum values noted through the sensitivity analysis. It is found that Case 3 operates at higher capacity (500 TPD) with lower SEC and higher COP than in Case 1 and Case 2 by an average of 3.26 % and 4.40 %, respectively.

The optimal composition of MR2 that is presented in Table 7 contains 4.21 % of ammonia, which may freeze out and block the flow in HX3 and HX4. This is because the cryogenic temperatures of MR2 reach to less than -140 °C (at streams 29 and 34) while the triple point of ammonia is −77.65 °C. However, the flexible configuration of the proposed process enables us to change the refrigerant composition with minor effect on the energetic performance of the process. For instance, as shown in Table 8, ammonia is removed from the composition of MR2 alongside adjustment of MR1 which provide a SEC of 0.868 kWh/kgH2Feed. Although this value is 4.20 % higher than the best obtained SEC with ammonia at capacity of 500 TPD (0.833 kWh/kgH2Feed, See Table 7), it is only 0.7 % higher than ammonia-based case at capacity of 300 TPD (0.862 kWh/kgH2Feed). Furthermore, the SEC without ammonia in MR2 is lower than the best precooling process available in the literature

(reference SMR with SEC of 1.082 kWh/kgH2Feed. [33]) by 19.78 %. It is worth to confirm that the presence of ammonia in MR1 has no freezing out problem as the cryogenic temperature of MR1 reaches a minimum value of -58 °C (at stream 13), which is higher than the triple point of ammonia by about of 20 °C.

5. Conclusions

In this study, a novel, efficient, and large-scale hydrogen precooling system is developed using dual mixed refrigerant process rather than pure or single mixed refrigerant (SMR) processes available in the literature. The structure of the proposed DMR process integrates two refrigeration cycles. The first cycle precooled the feed hydrogen from 25 °C to -53 °C and the second cycle precooled it to -192 °C at constant pressure of 21 bar. Also, using a systematic selection approach, heavyweight-based mixed refrigerant is developed for the first cycle (MR1), and lightweight-based mixed refrigerant is developed for the second refrigeration cycle (MR2). The performance of the new DMR

Table 7

Preliminary optimization for the compositions of MR1 and MR2, of the present DMR precooling process and their operational parameters.

Item	Case 1	Case 2	Case 3
Composition of MR1 (Molar fraction), [%]	Ethane: 10.00 %, Propane: 28.00 %, n-Pentane: 4.00 %, Ammonia: 28.00 %, Ethylene: 15.50 %, i-Pentane: 14.50 %	Ethane: 10.00 %, Propane: 28.00 %, n-Pentane: 4.00 %, Ammonia: 28.00 %, Ethylene: 15.50 %, i-Pentane: 14.50 %	Ethane: 10.00 %, Propane: 28.00 %, n-Pentane: 4.00 %, Ammonia: 28.00 %, Ethylene: 15.50 %, i-Pentane: 14.50 %
Composition of MR2 (Molar fraction), [%]	Methane: 38.03 %, Propane: 5.70 %, Nitrogen: 23.06 %, Ammonia: 4.21 %, Ethylene: 29.00 %	Methane: 38.15 %, Propane: 5.69 %, Nitrogen: 22.81 %, Ammonia: 4.21 %, Ethylene: 29.14 %	Methane: 38.15 %, Propane: 5.69 %, Nitrogen: 22.81 %, Ammonia: 4.21 %, Ethylene: 29.14 %
$\dot{m}_{HF}$, [TPD]	300	400	500
$\dot{m}_{HF}$, [kg/s]	3.47	4.63	5.79
$\dot{m}_{MR1}$, [kg/s]	48.00	66.00	84.80
$\dot{m}_{MR2}$, [kg/s]	33.10	45.10	56.00
$P_{h,MR1}$, [bar]	11.90	11.90	11.90
$P_{h,MR2}$, [bar]	39.50	38.90	39.50
$P_{l,MR1}$, [bar]	3.10	3.10	3.20
$P_{l,MR2}$, [bar]	4.70	4.90	5.31
$\dot{W}_{MRC,total}$, [MW]	10.79	14.31	17.36
$Q_{HXs,total}$, [MW]	47.65	64.94	81.47
$Q_{CL,total}$, [MW]	21.56	28.67	35.33
COP	4.42	4.54	4.69
SEC, [kWh/ kgH$_{2Feed}$]	0.862	0.858	0.833

Table 8

Proposed composition for MR1 and MR2 without ammonia.

Components	Basic MR1	Basic MR2 (with ammonia)	Adjusted MR1	Adjusted MR2 (without ammonia)
Methane	0.000	38.030	0.00	38.00
Ethane	10.000	0.000	11.80	4.00
Propane	28.000	5.700	27.20	6.70
n-Pentane	4.000	0.000	5.00	0.00
Nitrogen	0.000	23.060	0.00	23.10
Ammonia	28.000	4.2100	28.00	0.00
Ethylene	15.500	29.000	14.00	27.00
i-Butane	0.000	0.000	0.00	1.20
i-Pentane	14.500	0.000	14.00	0.00
$\dot{m}_{HF}$, [TPD]	300		300	
SEC, [kWh/ kgH$_{2Feed}$]	0.862		0.868	
$\dot{m}_{MR1}$, [kg/s]	48.00		49.00	
$\dot{m}_{MR2}$, [kg/s]	33.10		35.30	

precooling process is analyzed from energetic, exergetic, and economic point of views. Furthermore, detailed comparison with the most competitive reference SMR precooling process introduced by Sadaghiani and Mehrpooya [33] is performed. The main conclusions of the present study can be summarized as:

- Compared to the reference SMR precooling process, the proposed DMR process reduces the specific energy consumption (SEC) by 20.33 %, improves the coefficient of performance (COP) by 14.47 %, and reduced the total annualized cost by 12.24 %.

- The proposed DMR process can handle hydrogen precooling process at large scale ranging from 100 TPD to 1000 TPD with almost constant SEC of 0.862 kWh/kgH$_{2Feed}$.
- The exergetic performance of the proposed process (68.02 %) is slightly higher than of the reference SMR process (67.53 %). Further exergetic improvements can be achieved by optimizing the operating conditions of the heat exchangers and coolers.
- Increasing the higher-pressure for the new mixed refrigerants above their optimum values yields liquid phase at the entrance of the compressor.
- Increasing the low-pressure of the new mixed refrigerants above their optimum values yields temperature-cross problem in the heat exchangers.
- Compared to the pure-refrigerant precooling processes, the SEC of the present DMR process is reduced by more than 60.0 %.

Also, there is a trade-off between the SEC and the COP of the present DMR process. Therefore, further future rigorous optimization analysis is needed to optimize the operating conditions in order to achieve lower SEC, higher COP, at higher process capacity. Furthermore, the potential of applying the DMR configuration on the liquefaction part of the hydrogen liquefaction process is to be investigated as a future work.

CRediT authorship contribution statement

Ahmad K. Sleiti: Conceptualization, Investigation, Writing – original draft, Writing – review & editing, Resources, Formal analysis, Project administration, Funding acquisition, Supervision. **Wahib A. Al-Ammari:** Conceptualization, Writing – original draft, Investigation, Software, Data curation, Validation, Formal analysis. **Saud Ghani:** Writing – review & editing, Resources, Formal analysis, Supervision.

Declaration of competing interest

The authors declare that they have no known competing financial interests or personal relationships that could have appeared to influence the work reported in this paper.

Data availability

Data will be made available on request.

Appendix A. Supplementary data

Supplementary data to this article can be found online at https://doi.org/10.1016/j.est.2023.107471.

References

[1] M. Otto, K.L. Chagoya, R.G. Blair, S.M. Hick, J.S. Kapat, Optimal hydrogen carrier: holistic evaluation of hydrogen storage and transportation concepts for power generation, aviation, and transportation, J. Energy Storage 55 (2022), 105714, https://doi.org/10.1016/j.est.2022.105714.

[2] J. Incer-Valverde, L.J. Patiño-Arévalo, G. Tsatsaronis, T. Morosuk, Hydrogen-driven power-to-X: state of the art and multicriteria evaluation of a study case, Energy Convers. Manag. (2022) 266, https://doi.org/10.1016/j.enconman.2022.115814.

[3] M.G. Rasul, M.A. Hazrat, M.A. Sattar, M.I. Jahirul, M.J. Shearer, The future of hydrogen: challenges on production, storage and applications, Energy Convers. Manag. 272 (2022), 116326, https://doi.org/10.1016/j.enconman.2022.116326.

[4] Hydrogen Council, Hydrogen for Net-Zero. A Critical Cost-Competitive Energy Vector, 2021.

[5] F. Eljack, M.-K. Kazi, Prospects and challenges of green hydrogen economy via multi-sector global symbiosis in Qatar, Front. Sustain. 1 (2021) 1–15, https://doi.org/10.3389/frsus.2020.612762.

[6] M. Bailera, N. Kezibri, L.M. Romeo, S. Espatolero, P. Lisbona, C. Bouallou, Future applications of hydrogen production and CO2 utilization for energy storage: hybrid power to gas-oxycombustion power plants, Int. J. Hydrog. Energy 42 (2017) 13625–13632, https://doi.org/10.1016/j.ijhydene.2017.02.123.

[7] H. Nazir, N. Muthuswamy, C. Louis, S. Jose, J. Prakash, M.E. Buan, et al., Is the H2 economy realizable in the foreseeable future? Part II: H2 storage, transportation, and distribution, Int. J. Hydrog. Energy 45 (2020) 20693–20708, https://doi.org/10.1016/j.ijhydene.2020.05.241.

[8] D. Hjeij, Y. Biçer, M. Koç, Hydrogen strategy as an energy transition and economic transformation avenue for natural gas exporting countries: Qatar as a case study, Int. J. Hydrog. Energy 47 (2022) 4977–5009, https://doi.org/10.1016/j.ijhydene.2021.11.151.

[9] S.S. Mukherjee, H.A. Meshram, D. Rakshit, B.B. Saha, A comparative study of sensible energy storage and hydrogen energy storage apropos to a concentrated solar thermal power plant, J. Energy Storage 61 (2023), 106629, https://doi.org/10.1016/j.est.2023.106629.

[10] B. Ghorbani, S. Zendehboudi, Jouybari A. Khatami, Thermo-economic optimization of a hydrogen storage structure using liquid natural gas regasification and molten carbonate fuel cell, J. Energy Storage 52 (2022), 104722, https://doi.org/10.1016/j.est.2022.104722.

[11] A. Naquash, M.A. Qyyum, S. Min, S. Lee, M. Lee, Carbon-dioxide-precooled hydrogen liquefaction process: an innovative approach for performance enhancement–energy, exergy, and economic perspectives, Energy Convers. Manag. 251 (2022), 114947, https://doi.org/10.1016/j.enconman.2021.114947.

[12] S. Krasae-in, J.H. Stang, P. Neksa, Development of large-scale hydrogen liquefaction processes from 1898 to 2009, Int. J. Hydrog. Energy 35 (2010) 4524–4533, https://doi.org/10.1016/j.ijhydene.2010.02.109.

[13] D.O. Berstad, J.H. Stang, P. Nekså, Large-scale hydrogen liquefier utilising mixed-refrigerant pre-cooling, Int. J. Hydrog. Energy 35 (2010) 4512–4523, https://doi.org/10.1016/j.ijhydene.2010.02.001.

[14] N.M. Garceau, J.H. Baik, C.M. Lim, S.Y. Kim, I.H. Oh, S.W. Karng, Development of a small-scale hydrogen liquefaction system, Int. J. Hydrog. Energy 40 (2015) 11872–11878, https://doi.org/10.1016/j.ijhydene.2015.06.135.

[15] L. Yin, Y. Ju, Process optimization and analysis of a novel hydrogen liquefaction cycle, Int. J. Refrig. 110 (2020) 219–230, https://doi.org/10.1016/j.ijrefrig.2019.11.004.

[16] Y.E. Yuksel, M. Ozturk, I. Dincer, Analysis and assessment of a novel hydrogen liquefaction process, Int. J. Hydrog. Energy 42 (2017) 11429–11438, https://doi.org/10.1016/j.ijhydene.2017.03.064.

[17] J. Incer-Valverde, J. Mörsdorf, T. Morosuk, G. Tsatsaronis, Power-to-liquid hydrogen: exergy-based evaluation of a large-scale system, Int. J. Hydrog. Energy (2021), https://doi.org/10.1016/j.ijhydene.2021.09.026.

[18] S. Faramarzi, S.M.M. Nainiyan, M. Mafi, R. Ghasemiasl, A novel hydrogen liquefaction process based on LNG cold energy and mixed refrigerant cycle, Int. J. Refrig. 131 (2021) 263–274, https://doi.org/10.1016/j.ijrefrig.2021.07.022.

[19] J. Yang, Y. Li, H. Tan, J. Bian, X. Cao, Optimization and analysis of a hydrogen liquefaction process integrated with the liquefied natural gas gasification and organic Rankine cycle, J. Energy Storage 59 (2023), 106490, https://doi.org/10.1016/j.est.2022.106490.

[20] L. Yin, Y. Ju, Review on the design and optimization of hydrogen liquefaction processes, Front. Energy 14 (2020) 530–544, https://doi.org/10.1007/s11708-019-0657-4.

[21] H.-M. Chang, Park M. Gyun, Cascade JT systems with single-component refrigerants for hydrogen liquefaction, Cryogenics (Guildf.) 121 (2021), 103410, https://doi.org/10.1016/j.cryogenics.2021.103410.

[22] S. Krasae-In, Optimal operation of a large-scale liquid hydrogen plant utilizing mixed fluid refrigeration system, Int. J. Hydrog. Energy 39 (2014) 7015–7029, https://doi.org/10.1016/j.ijhydene.2014.02.046.

[23] M. Asadnia, M. Mehrpooya, A novel hydrogen liquefaction process configuration with combined mixed refrigerant systems, Int. J. Hydrog. Energy 42 (2017) 15564–15585, https://doi.org/10.1016/j.ijhydene.2017.04.260.

[24] B. Ghorbani, M. Mehrpooya, M. Amidpour, A novel integrated structure of hydrogen purification and liquefaction using natural gas steam reforming, organic Rankine cycle and photovoltaic panels, Cryogenics (Guildf.) 119 (2021), 103352, https://doi.org/10.1016/j.cryogenics.2021.103352.

[25] P. Pakzad, M. Mehrpooya, A. Zaitsev, Thermodynamic assessments of a novel integrated process for producing liquid helium and hydrogen simultaneously, Int. J. Hydrog. Energy 46 (2021) 37939–37964, https://doi.org/10.1016/j.ijhydene.2021.09.046.

[26] A. Naquash, M.A. Qyyum, M. Islam, N.R. Sial, S. Min, S. Lee, et al., Performance enhancement of hydrogen liquefaction process via absorption refrigeration and organic rankine cycle-assisted liquid air energy system, Energy Convers. Manag. 254 (2022), 115200, https://doi.org/10.1016/j.enconman.2021.115200.

[27] D. Lee, D. Quarme Gbadago, Y. Jo, G. Hwang, Y. Jo, R. Smith, et al., Integrating hydrogen liquefaction with steam methane reforming and CO2 liquefaction processes using techno-economic perspectives, Energy Convers. Manag. 245 (2021), 114620, https://doi.org/10.1016/j.enconman.2021.114620.

[28] A. Ebrahimi, M.H.M. Saharkhiz, B. Ghorbani, Thermodynamic investigation of a novel hydrogen liquefaction process using thermo-electrochemical water splitting cycle and solar collectors, Energy Convers. Manag. 242 (2021), 114318, https://doi.org/10.1016/j.enconman.2021.114318.

[29] B. Ghorbani, M.H. Hamedi, R. Shirmohammadi, M. Hamedi, M. Mehrpooya, Exergoeconomic analysis and multi-objective pareto optimization of the C3MR liquefaction process, Sustain. Energy Technol. Assess. 17 (2016) 56–67, https://doi.org/10.1016/j.seta.2016.09.001.

[30] H. Ansarinasab, M. Mehrpooya, Advanced exergoeconomic analysis of a novel process for production of LNG by using a single effect absorption refrigeration cycle, Appl. Therm. Eng. 114 (2017) 719–732, https://doi.org/10.1016/j.applthermaleng.2016.12.003.

[31] J. Stang, P. Nekså, E. Brendeng, On the design of an effient hydrogen liquefaction process, in: 16th World Hydrog Energy Conf 2006, WHEC 2006 2, 2006, pp. 1480–1485.

[32] S. Krasae-In, J.H. Stang, P. Neksa, Simulation on a proposed large-scale liquid hydrogen plant using a multi-component refrigerant refrigeration system, Int. J. Hydrog. Energy 35 (2010) 12531–12544, https://doi.org/10.1016/j.ijhydene.2010.08.062.

[33] M.S. Sadaghiani, M. Mehrpooya, Introducing and energy analysis of a novel cryogenic hydrogen liquefaction process configuration, Int. J. Hydrog. Energy 42 (2017) 6033–6050, https://doi.org/10.1016/j.ijhydene.2017.01.136.

[34] A. Riaz, M.A. Qyyum, S. Min, S. Lee, M. Lee, Performance improvement potential of harnessing LNG regasification for hydrogen liquefaction process: energy and exergy perspectives, Appl. Energy 301 (2021), 117471, https://doi.org/10.1016/j.apenergy.2021.117471.

[35] G. Skaugen, D. Berstad, Ø. Wilhelmsen, Comparing exergy losses and evaluating the potential of catalyst-filled plate-fin and spiral-wound heat exchangers in a large-scale Claude hydrogen liquefaction process, Int. J. Hydrog. Energy 45 (2020) 6663–6679, https://doi.org/10.1016/j.ijhydene.2019.12.076.

[36] H. Ansarinasab, M. Mehrpooya, A. Mohammadi, Advanced exergy and exergoeconomic analyses of a hydrogen liquefaction plant equipped with mixed refrigerant system, J. Clean. Prod. 144 (2017) 248–259, https://doi.org/10.1016/j.jclepro.2017.01.014.

[37] H. Ansarinasab, M. Mehrpooya, M. Sadeghzadeh, An exergy-based investigation on hydrogen liquefaction plant-exergy, exergoeconomic, and exergoenvironmental analyses, J. Clean. Prod. 210 (2019) 530–541, https://doi.org/10.1016/j.jclepro.2018.11.090.

[38] M.A. Qyyum, A. Riaz, A. Naquash, J. Haider, K. Qadeer, A. Nawaz, et al., 100% saturated liquid hydrogen production: mixed-refrigerant cascaded process with two-stage ortho-to-para hydrogen conversion, Energy Convers. Manag. 246 (2021), 114659, https://doi.org/10.1016/j.enconman.2021.114659.

[39] Ø. Wilhelmsen, D. Berstad, A. Aasen, P. Nekså, G. Skaugen, Reducing the exergy destruction in the cryogenic heat exchangers of hydrogen liquefaction processes, Int. J. Hydrog. Energy 43 (2018) 5033–5047, https://doi.org/10.1016/j.ijhydene.2018.01.094.

[40] AK Sleiti WA Al-Ammaria . Dual-mixed refrigerant precooling process. US 63/336,565 Provisional Patent, 2022.

[41] H. Rezaie Azizabadi, M. Ziabasharhagh, M. Mafi, Applicability of the common equations of state for modeling hydrogen liquefaction processes in Aspen HYSYS, Gas Process. J. 9 (2021) 11–28. 10.22108/gpj.2020.123736.1087.

[42] Y. Bi, L. Yin, T. He, Y. Ju, Optimization and analysis of a novel hydrogen liquefaction process for circulating hydrogen refrigeration, Int. J. Hydrog. Energy 47 (2022) 348–364, https://doi.org/10.1016/j.ijhydene.2021.10.012.

[43] H.-M.M. Chang, M.G. Park, M. Gyun Park, M.G. Park, Cascade JT systems with single-component refrigerants for hydrogen liquefaction, Cryogenics (Guildf.) 121 (2022), 103410, https://doi.org/10.1016/j.cryogenics.2021.103410.

[44] A. Naquash, A. Riaz, M. Abdul Qyyum, G. Kim, M. Lee, Process knowledge inspired opportunistic approach for thermodynamically feasible and efficient design of hydrogen liquefaction process, Int. J. Hydrog. Energy (2022), https://doi.org/10.1016/j.ijhydene.2022.11.163.

[45] A.K. Sleiti, W. Al-Ammari, S. Ahmed, J. Kapat, Direct-fired oxy-combustion supercritical-CO2 power cycle with novel preheating configurations -thermodynamic and exergoeconomic analyses, Energy 226 (2021), 120441, https://doi.org/10.1016/j.energy.2021.120441.

[46] F. Gharagheizi, M. Mehrpooya, Prediction of standard chemical exergy by a three descriptors QSPR model, Energy Convers. Manag. 48 (2007) 2453–2460, https://doi.org/10.1016/j.enconman.2007.04.005.

[47] M. Mehrpooya, S.A. Mousavi, M. Delpisheh, A. Zaitsev, A. Nikitin, 4E assessment and 3D parametric analysis of an innovative liquefied natural gas production process assisted by a diffusion–absorption refrigeration unit, Chem. Pap. 76 (2022) 5231–5252, https://doi.org/10.1007/s11696-022-02227-8.

[48] M. Saedi, M. Mehrpooya, M. Delpisheh, A. Zaitsev, Proposal and energy/exergy analysis of a novel cryogenic air separation configuration for the production of neon and argon, Chem. Pap. 76 (2022) 7075–7093, https://doi.org/10.1007/s11696-022-02396-6.

[49] A.K. Sleiti, W.A. Al-ammari, R. Arshad, Mekkawy T. El, Energetic, economic, and environmental analysis of solid oxide fuel cell-based combined cooling, heating, and power system for cancer care hospital, Build. Simul. 15 (2022) 1437–1454. https://doi.org/10.1007/s12273-021-0865-9.